3456 *Biochemistry* **2010,** *49,* 3456–3463
DOI: 10.1021/bi100128h

BIOCHEMISTRY
including biophysical chemistry & molecular biology
Article

Myelin Basic Protein and Myelin Protein 2 Act Synergistically to Cause Stacking of Lipid Bilayers[†]

Swetha Suresh,[‡] Chaozhan Wang,[§] Rahul Nanekar,[§] Petri Kursula,[§,#] and J. Michael Edwardson*[,‡]

[‡]*Department of Pharmacology, University of Cambridge, Tennis Court Road, Cambridge CB2 1PD, United Kingdom,* [§]*Department of Biochemistry, University of Oulu, Oulu, Finland, and* [#]*CSSB-HZI, DESY, Hamburg, Germany*

Received January 27, 2010; Revised Manuscript Received March 15, 2010

ABSTRACT: Saltatory conduction of nerve impulses along axonal membranes depends on the presence of a multilayered membrane, myelin, that wraps around the axon. Myelin basic protein (MBP) and myelin protein 2 (P2) are intimately involved in the generation of the myelin sheath. They are also implicated in a number of neurological diseases, including autoimmune diseases of both the central and peripheral nervous systems. Here, we have used atomic force microsopy (AFM) to study the effects of MBP and P2 on lipid bilayers. MBP in association with a mica substrate appeared unstructured, and tended to coat the mica surface in the form of a monolayer. In contrast, P2 appeared as discrete particles, with molecular volumes consistent with the formation of both monomers and dimers. Either MBP or P2, at micromolar concentrations, caused stacking of brain lipid bilayers. This stacking effect was significantly potentiated when both proteins were added together. Bilayers composed of phosphatidylcholine (PC) and phosphatidylserine (PS) were stacked by MBP, provided that cholesterol was also present; in contrast, P2 did not stack PC/PS/cholesterol bilayers. Hence, the bilayer stacking effects of the two proteins have different lipid requirements.

Myelin is a tightly packed, multilayered membrane system wrapped around selected axons in both the central and peripheral nervous systems (CNS and PNS, respectively). The main function of myelin is to contribute toward a 100-fold increase in the speed of the nerve impulse along the axon; myelin affects conduction speed both by acting as an insulator and by directing the localization of neuronal ion channels to the nodes of Ranvier.

Biochemically, myelin is a highly specialized domain of the glial cell plasma membrane. It contains approximately 80% lipid and 20% protein, and has little aqueous solvent. The major proteins found in myelin are unique to the myelin sheath, and are not found in significant amounts in other tissues; furthermore, the protein composition of CNS and PNS myelin is significantly different. Practically all of the myelin-specific proteins interact intimately with membranes, being either integral or peripheral membrane proteins.

In the region of compact myelin, only two non-transmembrane proteins are present in high abundance: the myelin basic protein (MBP)[1] and myelin protein 2 (P2). Both MBP and P2 are localized at the cytoplasmic apposition of two consecutive layers of the myelin membrane, where, in theory, they could be interacting with two membrane surfaces simultaneously. While the membrane binding of MBP (*1*−*11*) and P2 (*12*) has been studied previously, the detailed mechanisms of protein−membrane interactions, and their contribution to the overall myelin structure, are to a large extent still unknown. Furthermore, the possibility of a concerted action by the two proteins has not been addressed.

MBP is an intrinsically disordered molecule in aqueous solution, with a variety of splice isoforms and post-translational modifications in vivo. The major isoform in adult myelin is the 18.5-kDa form. Of its charge isomers, C1 and C8 have previously been expressed recombinantly in *Escherichia coli* (*13*, *14*) and characterized extensively in vitro. While C1 corresponds to the least modified form of MBP, C8 mimics the form seen, for example, in aggressive multiple sclerosis (*4*). MBP is one of the major autoantigens in multiple sclerosis, and has a very high positive charge, which contributes to its intimate membrane interactions.

P2 is a small lipid-binding protein (*15*) found predominantly in the PNS myelin sheath. While its crystal structure has been characterized (*16*), no detailed functional information exists on its role in myelin. The surface of P2 has a high positive charge, which is likely to be crucial to its interaction with the negatively charged inner leaflet of the myelin membrane. The function of P2 is likely related both to the integrity of the myelin multilayer, and to lipid transport to and from the membrane. P2 is a candidate autoantigen in the peripheral autoimmune neuropathy, Guillain-Barré syndrome (*17*). We have recently shown, using neutron scattering methods, that P2 has a stabilizing effect on membrane dynamics (*18*).

Here, we have used atomic force microscopy (AFM) to address the membrane interactions of MBP and P2. Both MBP and P2, on binding to the membrane surface, induced the stacking of membrane bilayers. Interestingly, the stacking was more efficient when both proteins were present. Overall charge affected the

[†]This work was supported by the Academy of Finland (P.K.) and the Sigrid Juselius Foundation (Finland) (P.K.). S.S. is supported by a Cambridge Nehru Fellowship and a Cambridge Overseas Research Studentship.

*To whom correspondence should be addressed. Phone: 44-1223-334014. Fax: 44-1223-334100. E-mail: jme1000@cam.ac.uk.

[1]Abbreviations: AFM, atomic force microscopy; CNS, central nervous system; HBS, Hepes-buffered saline; MBP, myelin basic protein; PC, phosphatidylcholine; PLP, proteolipid protein; PNS, peripheral nervous system; PS, phosphatidylserine; P2, myelin protein 2; SM, sphingomyelin.

 Published on Web 03/25/2010

stacking of the membranes by MBP, and variation in the lipid composition of the membrane affected MBP and P2 differently. These observations are highly relevant to the understanding of the formation of the multilayered, tightly packed myelin sheath in vertebrates.

EXPERIMENTAL PROCEDURES

Purification of MBP and P2. Recombinant mouse MBP C1 and C8 isoforms were expressed and purified as His-tagged versions, essentially as described previously (*13*, *14*), with minor modifications. Briefly, cells from a 1-L culture were suspended in 20 mL lysis buffer (6 M urea, 300 mM NaCl, 10 mM imidazole, 50 mM Tris, pH 8.0) and disrupted by sonication in an ice−water bath. A 3-mL Ni-NTA agarose column was equilibrated by 10 column volumes of lysis buffer. After the sample was loaded, the column was washed with at least 10 column volumes of washing buffer (6 M urea, 300 mM NaCl, 20 mM imidazole, 50 mM Tris, pH 8.0). The protein was eluted using elution buffer (6 M urea, 300 mM NaCl, 250 mM imidazole, 50 mM Tris, pH 8.0). Urea was then removed by dialysis against 20 mM HEPES, pH 7.5 at 4 °C, and precipitates were removed by centrifugation.

Full-length human myelin P2 protein was expressed as a recombinant protein using the pTH27 vector, encoding an N-terminal His tag and a TEV protease cleavage site (*19*). For expression, *E. coli* Rosetta (pLysS) cells harboring the expression vector were transferred into 10 mL of complex autoinducing medium (*20*) with antibiotics (ampicillin 100 μg/mL and chloramphenicol 34 μg/mL), and the culture was grown overnight at 37 °C. Next morning, the 10-mL culture was transferred into 1 L of complex autoinducing medium with antibiotics. Growth was continued at 37 °C for 4 h and at 18 °C for 48 h. Then, the cells were collected by centrifugation and stored at −20 °C. For purification, cells from 2 L of culture were thawed, and 20 mL of lysis buffer (50 mM sodium phosphate, 300 mM NaCl, and 10 mM imidazole, pH 8.0) were added along with one Complete Mini EDTA-free tablet (Roche). The cells were disrupted by sonication on ice, and cell debris was removed by centrifugation. A Ni-NTA agarose column was equilibrated with lysis buffer, and the supernatant was applied onto the column. The column was washed with washing buffer (50 mM sodium phosphate, 300 mM NaCl, 20 mM imidazole, pH 8.0) until the A_{280} reached the baseline. Protein was then eluted in 2-mL fractions with elution buffer (50 mM sodium phosphate, 300 mM NaCl, and 250 mM imidazole, pH 8.0), and the fractions were checked for purity by SDS−polyacrylamide gel electrophoresis. TEV protease (*21*) was used to cleave the His tag overnight at 4 °C. The protein was further purified using size exclusion chromatography on a HiLoad 16/60 Superdex 75 column (GE Healthcare) using the Akta purifier (GE Healthcare). Equilibration was carried out with 120 mL of protein buffer (20 mM HEPES, 150 mM NaCl, 10% glycerol, pH 7.5). P2 was concentrated to 2 mL by centrifugation at 4 °C in an Amicon^R Ultracel 3K, and the concentrated protein was injected into the column. Fractions corresponding to the absorbance peak on the chromatogram were analyzed by SDS−polyacrylamide gel electrophoresis.

Atomic Force Microscopy. AFM imaging was performed using a Veeco Digital Instruments Multimode instrument (Swavesey, UK), controlled by a Nanoscope IIIa controller, and equipped with a J-scanner. Imaging in air was carried out in tapping mode, using commercial OMCL-AC160TS-E Si probes (Olympus), which have a resonance frequency of 300 kHz. $1 \times 1\ \mu m^2$ and $2 \times 2\ \mu m^2$ scans were recorded, with the z-limit at 1 μm. Imaging under fluid was carried out in tapping mode, using NSC-18 cantilevers with a Cr−Au coating (Mikromasch). Their resonant frequencies were 30−35 kHz. In both cases the rms voltage was maintained at 2 V. Set-point and drive amplitude were adjusted so that the samples could be imaged with the smallest possible force. Scanning frequencies were kept ∼5% below the maximal resonance peak. Scan rates were 2−4 Hz.

Imaging of Proteins on Mica. Muscovite mica (Agar Scientific, Stansted, UK) was cut into small discs and glued to AFM specimen discs (Agar Scientific) using cyanoacrylate glue. Proteins were serially diluted in BPC water (Sigma, Poole, UK) to a concentration where particles could be seen individually on mica (0.67 nM for MBP and 10 nM for P2). Samples (50 μL) were placed on freshly cleaved mica for 15 min. Mica discs were washed extensively with BPC water to remove any unadsorbed protein, and then dried under a stream of nitrogen to remove all traces of moisture.

Imaging of Supported Lipid Bilayers. Egg L-α-phosphatidylcholine (PC), 1,2-dioleoyl-*sn*-glycero-3-phosphatidylserine (PS), cholesterol, porcine brain sphingomyelin (SM), and brain total lipid extract were obtained as chloroform stocks from Avanti Polar Lipids (Alabaster, AL). The following lipid mixtures (mole %) were produced, all at a final concentration of 2 mg/mL: brain total lipid extract, PC/PS (75%/25%), PC/PS/SM/cholesterol (45%/15%/30%/10%), PC/PS/SM (55%/15%/30%), and PC/PS/cholesterol (75%/15%/10%). The chloroform was evaporated using nitrogen gas and the lipids were rehydrated overnight with BPC water (Sigma). The lipids were vortexed to produce multilamellar liposomes, and then sonicated using a probe sonicator at an amplitude of 10 mA for 5−15 s to produce unilamellar liposomes. The liposomes were incubated on ice for 10−15 min before formation of bilayers. Mica discs were glued to AFM specimen discs using epoxy glue. Liposomes (50 μL) were added to the mica along with 50 μL of Hepes-buffered saline (HBS; 50 mM Hepes, pH 7.6, 150 mM NaCl) containing 1 mM $CaCl_2$ and left for 6−10 min before gentle washing with 2 mL of the same buffer to remove unadsorbed vesicles. Fresh buffer (150 μL) was placed on top of the lipid bilayer.

Protein-free bilayers were first imaged before addition of any protein. Proteins were added to the appropriate final concentration in 50 μL of HBS containing 1 mM $CaCl_2$. This buffer was exchanged with same volume of protein-free buffer in the fluid cell. After 10 min, the buffer in the fluid cell was exchanged with protein-free buffer.

Data Analysis. P2 particles tended to adopt the shape of a spherical cap. Using values obtained for radii and heights, molecular volumes were calculated using the formula

$$V_m = (\pi h/6)(3r^2 + h^2) \quad (1)$$

where h is the particle height and r is the radius (*22*). This volume was compared with the theoretical volume for a given molecular mass obtained using the formula

$$V_c = (M_0/N_0)(V_1 + dV_2) \quad (2)$$

where M_0 is the molecular mass, N_0 is Avogadro's number, V_1 and V_2 are the partial specific volumes of particle (0.74 cm^3/g; ref *23*) and water (1 cm^3/g), respectively, and d is the extent of protein hydration (taken as 0.4 g water/g protein; ref *24*).

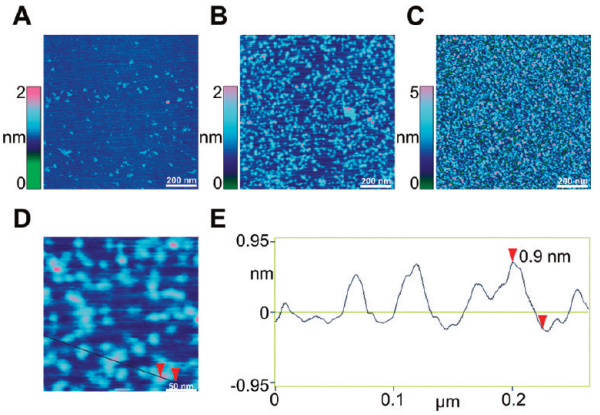

FIGURE 1: Association of MBP-C1 with mica. (A−C) Low-magnification AFM images of MBP-C1 at concentrations of 0.67 nM (A), 13.5 nM (B), and 54 nM (C). Color-height scales are shown at the left of each image. (D) Zoomed image from (B). (E) Section taken at the position indicated by the line in (D).

MBP had no particular shape when imaged on mica, consistent with previous reports that it has no intrinsic shape in solution (*25*). For this reason particle analysis was not attempted.

RESULTS

Purified MBP (C1 isoform) was first imaged in association with mica. As shown in Figure 1, MBP-C1 did not have a recognizable shape, but rather appeared in the form of amorphous particles that were considerably flattened on the mica substrate. Considerable self-association occurred, although no particular oligomerization state was detected. At the higher concentrations, the proteins coated the mica in the form of a fenestrated monolayer.

When liposomes composed of total brain lipids were allowed to collapse onto mica, the resulting supported lipid bilayer, imaged under fluid, was smooth and featureless, with many breaks that revealed the mica substrate (Figure 2A). A section through the bilayer (Figure 2B) indicated a bilayer thickness of 2.21 nm. This is thinner than the expected value of around 4 nm, which we have reported previously (e.g., ref *26*). We attribute this underestimation of bilayer thickness to a partial penetration of the bilayer caused by the rather stiff spring constant (3.5 N/m) of the Mikromasch NSC18 etched silicon probe used in these experiments, compared with a spring constant of 0.58 N/m for the Veeco DNP-S silicon nitride probe used previously. We used the stiff cantilevers because they permit stable imaging at a high frequency, enabling us to track rapid structural changes (reviewed in ref *27*). We have, in fact, directly compared the apparent bilayer thicknesses in a sample of an incompletely formed bilayer when visualized using the two different probes. A bilayer thickness of 4.0 nm was seen with the Veeco probe, as previously reported (*26*), while the Mikromasch probe gave an apparent thickness of 2.2−2.5 nm, as seen in the present study. Note also that the measured thickness varied with the lipid composition of the bilayer. For instance, the apparent thickness of a PC/PS/SM/cholesterol (45%/15%/30%/10%) bilayer was 3.79 nm, whereas a PC/PS (75%/25%) bilayer appeared to be only 2.00 nm thick (see below). This variability likely indicates differences in the "stiffness" of the various bilayers in addition to real differences in bilayer thickness.

When MBP-C1 (3.6 μM) was added to the solution bathing the supported lipid bilayer shown in Figure 2A, raised features

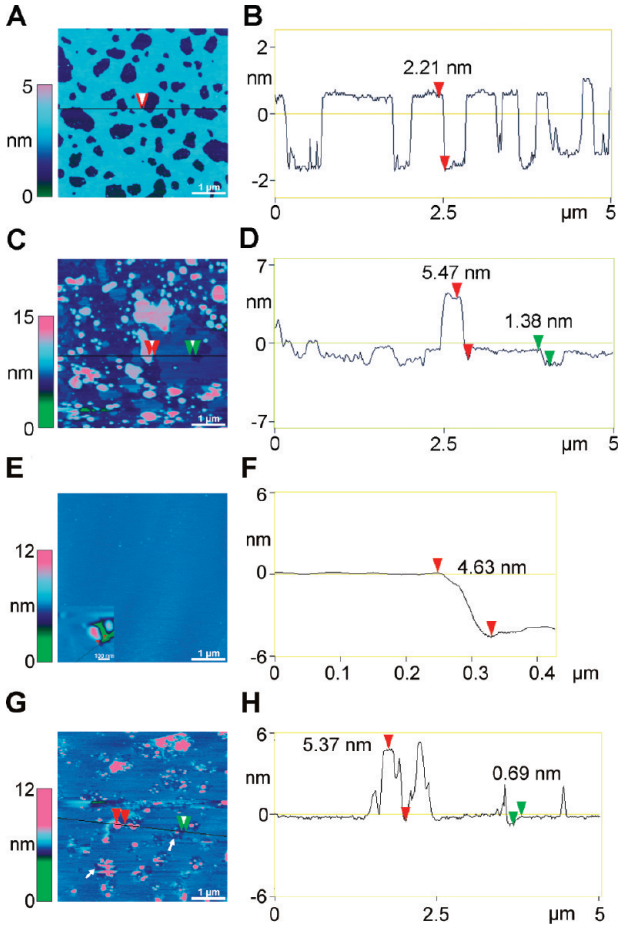

FIGURE 2: MBP-C1 induces stacking of brain lipid bilayers. (A) AFM image of a protein-free brain lipid bilayer. The lighter areas represent the surface of the bilayer, and the darker areas represent the mica substrate. A color-height scale is shown at the left. (B) Section through the bilayer taken at the position indicated by the line in (A). (C) AFM image of a bilayer that had been incubated with MBP-C1 (3.6 μM). MBP binds to the mica substrate as well as the bilayer. Note the difference in height scale compared with (A). (D) Section taken at the position indicated by the line in (C). Note the increased height compared with the section in (B), indicating bilayer stacking. (E) Image of protein-free dense mica coating composed of total brain lipids. The inset at bottom left is an area that has been scratched to demonstrate the presence of the lipid coating. (F) Section through the scratched area taken at the position indicated by the line in (E). (G) Image of a dense lipid coating that had been incubated with MBP-C1. Arrows indicate areas where the lipid had been depleted. (H) Section taken at the position indicated by the line in (G).

became apparent (Figure 2C). The section in Figure 2D shows that the step down from a single bilayer was reduced to 1.38 nm, likely because of the coating of the mica with MBP (see above). The section also indicates a raised feature of height 5.47 nm. No intermediate heights were seen, indicating that the higher level represents an additional bilayer, likely separated from the original bilayer by an MBP layer. Note that no new lipid was added to the sample, and, as expected, the total area of mica covered by bilayer fell after addition of MBP. Specifically, before addition of MBP, bilayers covered 74 ± 1% (n = 9) of the mica surface. After MBP addition, only 51 ± 3% (n = 9) of the mica was covered, although 10 ± 3% of the mica was now covered by a double bilayer. Hence, the total bilayer area (single plus double) fell from 74% to 61%, indicating some bilayer loss from the surface as a consequence of MBP addition.

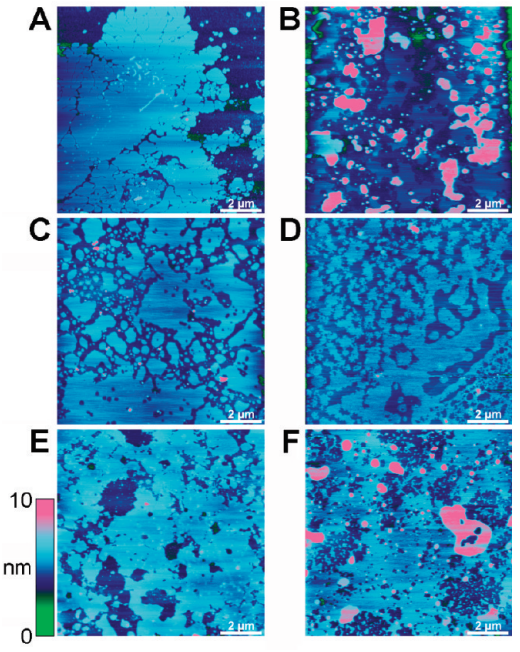

FIGURE 3: MBP-C8 is less effective than MBP-C1 at stacking bilayers. AFM images of brain lipid bilayers in the presence of 1.8 μM (A) or 3.6 μM (B) MBP-C1, or 1.8 μM (C), 3.6 μM (D), 9.0 μM (E), or 10.8 μM (F) MBP-C8. A color-height scale is shown at the left.

To exclude the possibility that MBP was bringing about its effect simply by causing desorption of the single bilayer from the mica, we added sufficient liposomes to completely coat the mica. Now the mica coating was featureless (Figure 2E), but deliberate "scratching" of the surface with the AFM tip (Figure 2E, inset) revealed that the coating was 4.63 nm thick (Figure 2F), likely indicating the presence of a double bilayer. After addition of MBP-C1 (3.6 μM) to this sample, raised features were again seen, consistent with bilayer stacking (Figure 2G,H). Depressions were also apparent in the surrounding lipid (arrows, Figure 2G). These were often adjacent to the raised features, suggesting that they represent the sites from which lipid was removed.

MBP-C8 is the least charged MBP isoform, and mimics the highly modified form found in aggressive cases of multiple sclerosis. To investigate the effect of charge on the behavior of MBP, we compared the abilities of MBP-C1 and MBP-C8 to cause bilayer stacking. Figure 3A,B shows the effects of MBP-C1 at concentrations of 1.8 and 3.6 μM, respectively. Bilayer stacking was minimal at 1.8 μM, but obvious at 3.6 μM, consistent with the results presented in Figure 2. In contrast, MBP-C8 caused minimal stacking at 1.8 μM (Figure 3C), 3.6 μM (Figure 3D), and 9.0 μM (Figure 3E), and stacking began only at 10.8 μM (Figure 3F). Hence, the reduction in charge in MBP-C8 causes a corresponding reduction in its ability to cause bilayer stacking.

In an attempt to pinpoint the lipid requirements for the bilayer stacking effect of MBP, we incubated supported bilayers of various defined compositions with MBP-C1 (3.6 μM). MBP was able to stack bilayers composed of PC/PS/SM and cholesterol (Figure 4). Note that in the absence of protein, these bilayers showed protruding areas (0.62 nm high in Figure 4B), which are likely to be SM/cholesterol-enriched domains (see ref *26*). MBP also stacked bilayers composed of PC/PS and cholesterol (Figure 5). However, no stacking was seen with bilayers composed of PC/PS and SM (Figure 6A) or just PC/PS (Figure 6B).

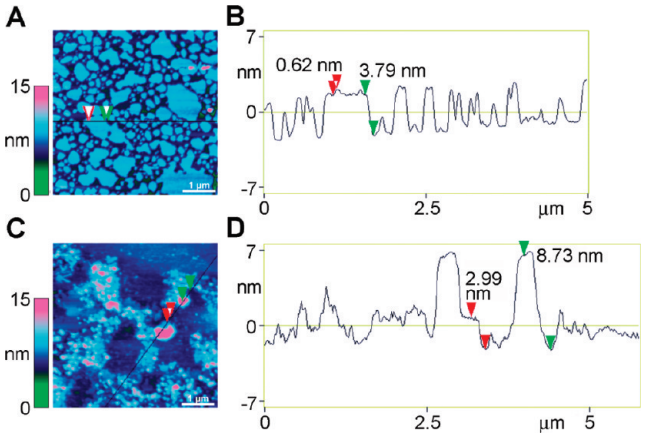

FIGURE 4: MBP-C1 induces stacking of bilayers composed of PC/PS/SM and cholesterol (45%/15%/30%/10%). (A) AFM image of a protein-free bilayer. A color-height scale is shown at the left. (B) Section through the bilayer taken at the position indicated by the line in (A). (C) AFM image of a bilayer that had been incubated with MBP-C1 (3.6 μM). (D) Section taken at the position indicated by the line in (C). Note the increased height compared with the section in (B), indicating bilayer stacking.

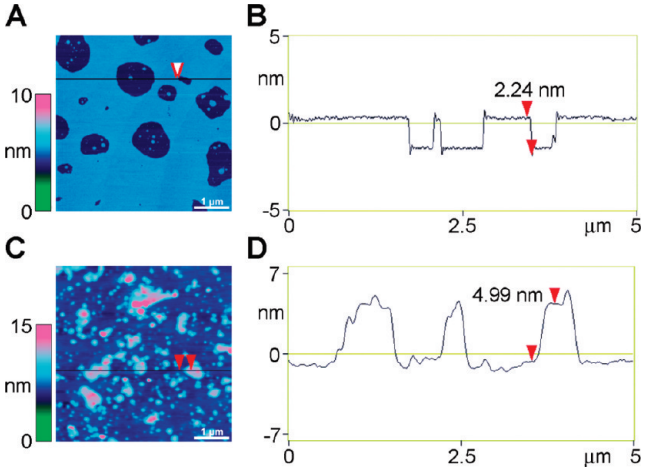

FIGURE 5: MBP-C1 induces stacking of bilayers composed of PC/PS and cholesterol (75%/15%/10%). (A) AFM image of a protein-free bilayer. A color-height scale is shown at the left. (B) Section through the bilayer taken at the position indicated by the line in (A). (C) AFM image of a bilayer that had been incubated with MBP (3.6 μM). Note the difference in height scale compared with (A). (D) Section taken at the position indicated by the line in (C). Note the increased height compared with the section in (B), indicating bilayer stacking.

These results indicate that cholesterol is required to support bilayer stacking by MBP.

When myelin protein P2 was imaged in association with mica (in air), a spread of particles was seen, most of which adopted the approximate shape of a spherical cap (Figure 7A, main panel). Close inspection revealed the presence of two particle sizes (Figure 7A, right-hand panels). Sections through two representative particles (Figure 7B) indicate differences in both diameter and height. The dimensions of a large number of particles were measured, and eq 1 was used to calculate their molecular volumes. A frequency distribution of molecular volumes is shown in Figure 7C. The distribution is well fitted by two Gaussian curves, which have volume peaks at 29 and 61 nm^3. The predicted molecular volume for a P2 monomer of molecular mass 14.8 kDa, according to eq 2, is 28 nm^3. Hence, the two volume peaks likely correspond to P2 monomers and dimers.

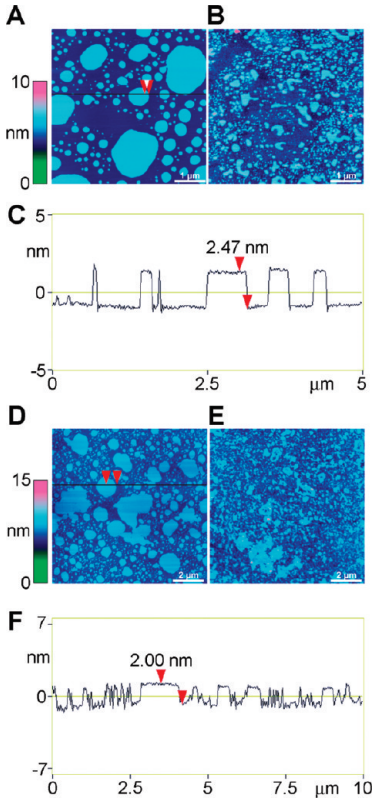

FIGURE 6: MBP-C1 does not induce bilayer stacking in the absence of cholesterol. (A) AFM image of a protein-free bilayer composed of PC/PS and SM (55%/15%/30%). A color-height scale is shown at the left. (B) AFM image of a bilayer that had been incubated with MBP (3.6 μM). (C) Section through the bilayer shown in (A) taken at the position indicated by the line. (D) AFM image of a protein-free bilayer composed of PC and PS (75%/25%). (E) AFM image of a PC/PS bilayer that had been incubated with MBP (3.6 μM). (F) Section through the bilayer shown in (D) taken at the position indicated by the line.

When brain lipid bilayers were exposed to MBP-C1 at a concentration of 1.8 μM, only a minimal amount of bilayer stacking was observed (Figure 8A). Myelin protein P2, at a concentration of 0.338 μM, also caused a small but detectable amount of bilayer stacking (Figure 8B). The section through the P2-exposed bilayer (Figure 8C) indicates the presence of a double bilayer on top of the lowest bilayer. Note that, as for MBP-C1, P2 was also able to stack bilayers after dense coating of the mica with lipid (data not shown). Significantly, when a bilayer was incubated with both MBP (1.8 μM) and myelin protein P2 (0.338 μM) extensive bilayer stacking was seen (Figure 8E), up to a maximum thickness of 11.15 nm.

In contrast to the result for MBP, the presence of cholesterol was not sufficient for bilayer stacking by myelin protein P2. Only single bilayers were observed either in PC/PS/SM bilayers in the presence of cholesterol (Figure 9A) or in PC/PS bilayers in the absence of cholesterol (Figure 9B).

DISCUSSION

We have used AFM to obtain detailed information on the membrane binding properties of two proteins specific to the myelin sheath of the vertebrate nervous system: MBP and P2. Both proteins bound to lipid bilayers and induced bilayer stacking. As discussed below, these observations increase our understanding of the formation and the overall structure and stability of myelin.

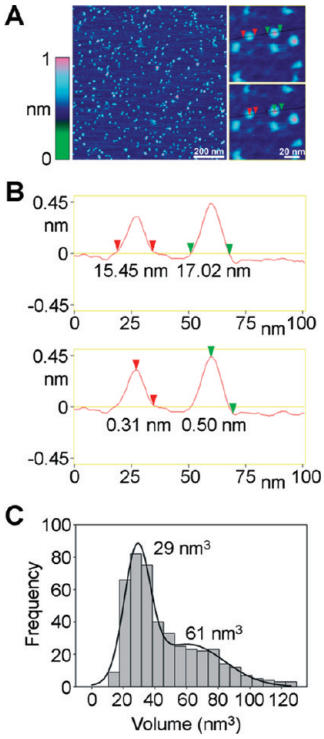

FIGURE 7: P2 associates with mica in the form of monomers and dimers. (A) The main panel shows a low-magnification AFM image of P2 bound to mica. A color-height scale is shown at the left. The insets (right-hand panels) are zoomed images of a region showing the presence of a monomer and a dimer. (B) Sections taken at the position indicated by the lines in (A), indicating the diameters (upper panel) and heights (lower panel) of two particles. (C) Frequency distribution of molecular volumes calculated for a population of P2 particles bound to mica. The curve indicates the two Gaussian functions that were fitted to the data. The peaks of the distributions are shown.

What are the factors involved in the formation and maintenance of the compacted myelin sheath? The compaction of myelin involves both the removal of cytoplasm and extracellular solvent from between the membranes, and the generation of tight interactions between turns of the membrane. X-ray diffraction analysis of tissue samples has shown that the repeat distance in myelin is around 18 nm. The extracellular spacing in myelin is 3−5 nm, and the intracellular space has been estimated to be around 3−4 nm (*28*). This implies that between the membranes, space is available only for small proteins or small domains. In principle, in the compacted regions of myelin, only two noninteral membrane proteins are present: MBP and P2. Their high concentration between the cytoplasmic faces of consecutive turns of the myelin membrane suggests that they intimately interact with the membrane surface in this domain, which contains little water. We have previously shown by neutron scattering that lipid bilayers made from synthetic lipids are stabilized by P2 (*18*). Our experiments here indicate that either MBP or P2 alone are able to cause bilayer stacking, proving that they are able to provide an adhesive force between stacked membrane layers. In earlier studies, different methods have also been used to observe vesicle aggregation and multilayer formation by the two proteins.

Both MBP and P2 have a high pI, and thus, have a large net positive charge at neutral pH. MBP is the more basic of the two proteins, with a pI near 11 in the absence of post-translational modifications. Interestingly, however, the concentration of P2 that was required to induce membrane stacking in the AFM experiment was much lower than that for MBP. Thus, charge

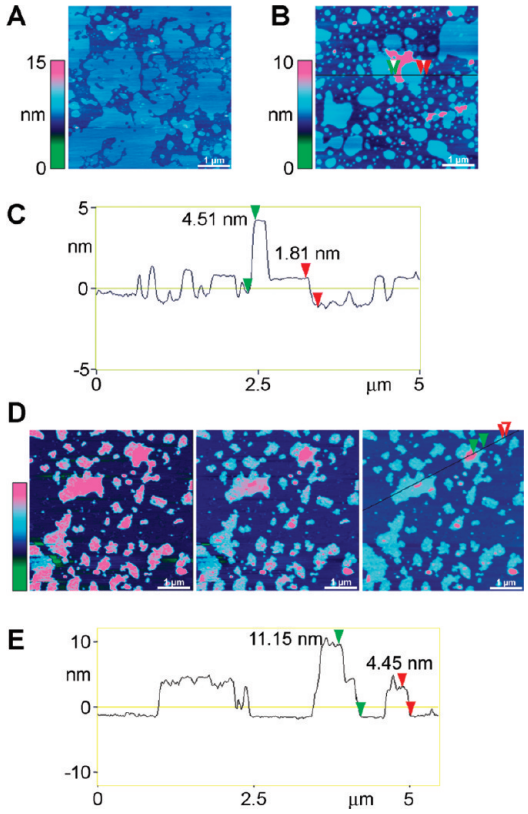

FIGURE 8: MBP-C1 and P2 act synergistically to cause bilayer stacking. (A) AFM image of a brain lipid bilayer that had been incubated with MBP (1.8 μM). A color-height scale is shown at the left. Note the reduced extent of bilayer stacking compared with that seen with 3.6 μM MBP (Figure 2). (B) AFM image of a brain lipid bilayer that had been incubated with P2 (0.338 μM). A color-height scale is shown at the left. (C) Section through the bilayer shown in (B) taken at the position indicated by the line. The heights indicate bilayer stacking. (D) AFM image of a brain lipid bilayer that had been incubated with both MBP (1.8 μM) and P2 (0.338 μM). The three panels show the same image with different shade-height scales, to reveal the extent of bilayer stacking. Left-hand panel: 0−10 nm; center panel: 0−15 nm; right-hand panel: 0−24 nm. (E) Section taken at the position indicated by the line in (D). Note the increase in heights compared with (C), indicating increased bilayer stacking with MBP plus P2.

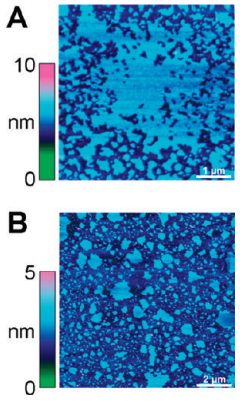

FIGURE 9: Cholesterol does not support bilayer stacking by P2. (A) AFM image of a bilayer composed of PC/PS/SM and cholesterol (45%/15%/30%/10%) that had been incubated with P2 (0.338 μM). A color-height scale is shown at the left. (B) AFM image of a bilayer composed of PC and PS (75%/25%) that had been incubated with P2 (0.338 μM). A color-height scale is shown at the left.

alone is not the driving factor for membrane stacking. P2 is a compactly folded protein (*16*), with a net positive surface charge. It is likely that the local high positive electrostatic potential on the P2 surface makes it functional in membrane stacking at even lower concentrations than MBP. On the other hand, the C8 isoform of MBP caused stacking only at higher concentrations, compared with C1, indicating that post-translational modifications in MBP may weaken its interaction with membranes, especially under circumstances where MBP is located between two membrane surfaces. Consistent with this interpretation, the least charged C8 isoform of MBP is found mainly in aggressive cases of multiple sclerosis, and in infants, where myelin is not fully compacted (*29*, *30*).

By making model membranes using pure synthetic lipids, further details on the membrane stacking process and its requirements were obtained. Our results indicate that while both MBP and P2 efficiently stack brain lipid bilayers, significant differences exist in their lipid requirements. Specifically, membrane stacking by MBP was supported by the presence of cholesterol, a component of detergent-insoluble membrane domains that is thought to provide additional rigidity to cellular membranes. In the context of myelination, it has been shown that the availability of cholesterol is rate-limiting for myelin membrane synthesis (*31*). On the other hand, P2 was unable to stack membranes made of PC, PS, and SM in the presence of cholesterol, or PC and PS in the absence of cholesterol, indicating additional requirements for P2 function. One possibility is that the monomeric lipid bound inside the barrel structure of P2 may have an effect on its membrane attachment properties. The localization of P2 with respect to membrane microdomains has not been studied, but all myelin lipids, including cholesterol, have been shown to copurify with P2 from the bovine PNS (*32*). In vesicle aggregation and binding studies, it has previously been shown that cholesterol enhances the lipid interactions of MBP (*33*−*35*). Recent evidence also suggests that the binding of MBP to cholesterol-containing membranes affects the formation of lipid microdomains (*36*, *37*), and that MBP localizes to detergent-resistant, cholesterol-rich microdomains (*38*−*40*). Thus, MBP specifically interacts with cholesterol-rich membrane domains, such as those found in myelin, and is functionally capable of stacking such membranes.

Interestingly, there is apparent synergy between MBP and P2 in membrane stacking. Since the two proteins localize to the same compartment in compact myelin in vivo, this observation suggests that MBP and P2 work together in the formation and maintenance of the compacted myelin structure. In this respect, it is interesting to note that while MBP is present in both the CNS and PNS, it is much more highly concentrated in CNS myelin. P2, on the other hand, is almost exclusively found in PNS myelin at a high concentration, although it is also detectable in CNS myelin (*41*). Thus, the concentration of MBP and P2 combined is rather similar in CNS and PNS, providing an explanation for the similar compaction of the myelin sheath despite the differing protein composition between the two branches of the nervous system. It has been suggested that an optimal ratio of MBP to negatively charged lipid on the membrane is such that each basic residue in MBP binds to a negative lipid (*11*). On the other hand, the binding of P2 to lipid vesicles was found to saturate at 15% protein, which corresponds to the amount of P2 found in PNS myelin (*12*). Naturally, on the extracellular side of the myelin membrane leaflets, different proteins, such as P0 in the PNS and proteolipid protein (PLP) in the CNS, also play major roles in maintaining myelin structure.

In the case of MBP, one of the best-characterized model systems is the shiverer mouse, which has a deficiency in

MBP (*42*). As a result, CNS myelin of this mutant is strongly diminished and poorly compacted (*43*). On the other hand, PNS myelin of the shiverer appears normal, although MBP is missing. In this respect, it is important to note that P2 has been shown to be present in shiverer PNS myelin (*44*, *45*), suggesting a role in PNS myelin compaction. In addition, a significantly decreased expression level of P2 has been detected in a case of congenital hypomyelination neuropathy (*46*), although the significance of this finding has not been fully elucidated. Thus, current evidence points toward a scenario, in which MBP alone would be crucial for myelin compaction in the CNS, while MBP and P2 may act together in the PNS.

Structurally, MBP and P2 are different, despite their high positive charge and similar localization. MBP is one of the best-characterized intrinsically unstructured proteins, although it is known to show at least local folding upon ligand binding. The heterogeneous nature of the MBP particles seen by AFM supports the idea that MBP has no single defined 3D structural state. AFM has also previously been used to show that MBP behaves differently when bound to a membrane, when compared to mica-bound MBP (*6*). P2, on the other hand, is a compactly folded protein, thought to be monomeric in solution. The presence of myelin lipids has been suggested to affect P2 structure (*32*). While the main particle species seen for P2 corresponded to this form, a potential dimeric form was also seen. A remaining question relates to the role to the P2 dimer particles seen in the AFM images in membrane stacking. Our recombinant system for obtaining human P2 and its mutated variants will shed further light on the structure−function relationships of P2 in the future.

Taken together, our results show that the myelin-specific proteins MBP and P2 both bind to brain lipid bilayers and induce their stacking. Stacking is affected by at least three factors: the charge of MBP (likely linked to its state of post-translational modification), the synergy between MBP and P2, and the lipid composition of the membrane. Additional factors could include the folding and dimerization of P2, and the binding of different monomeric lipid molecules inside P2. Considering the results from our reductionist approach here and in the earlier literature, we believe that P2 and its observed synergy with MBP play a role in the formation of normally compacted myelin, especially in the PNS.

REFERENCES

1. Persaud, R., Boggs, J. M., Wood, D. D., and Moscarello, M. A. (1989) Interaction of glycosylated human myelin basic protein with lipid bilayers. *Biochemistry 28*, 4209–4216.
2. Jo, E., and Boggs, J. M. (1995) Aggregation of acidic lipid vesicles by myelin basic protein: dependence on potassium concentration. *Biochemistry 34*, 13705–13716.
3. Boggs, J. M., Yip, P. M., Rangaraj, G., and Jo, E. (1997) Effect of posttranslational modifications to myelin basic protein on its ability to aggregate acidic lipid vesicles. *Biochemistry 36*, 5065–5071.
4. Beniac, D. R., Wood, D. D., Palaniyar, N., Ottensmeyer, F. P., Moscarello, M. A., and Harauz, G. (1999) Marburg's variant of multiple sclerosis correlates with a less compact structure of myelin basic protein. *Mol. Cell Biol. Res. Commun. 1*, 48–51.
5. Boggs, J. M., Rangaraj, G., Koshy, K. M., Ackerley, C., Wood, D. D., and Moscarello, M. A. (1999) Highly deiminated isoform of myelin basic protein from multiple sclerosis brain causes fragmentation of lipid vesicles. *J. Neurosci. Res. 57*, 529–535.
6. Mueller, H., Butt, H. J., and Bamberg, E. (1999) Force measurements on myelin basic protein adsorbed to mica and lipid bilayer surfaces done with the atomic force microscope. *Biophys. J. 76*, 1072–1079.
7. Boggs, J. M., and Rangaraj, G. (2000) Interaction of lipid-bound myelin basic protein with actin filaments and calmodulin. *Biochemistry 39*, 7799–7806.
8. Ishiyama, N., Bates, I. R., Hill, C. M., Wood, D. D., Matharu, P., Viner, N. J., Moscarello, M. A., and Harauz, G. (2001) The effects of deimination of myelin basic protein on structures formed by its interaction with phosphoinositide-containing lipid monolayers. *J. Struct. Biol. 136*, 30–45.
9. Bates, I. R., Boggs, J. M., Feix, J. B., and Harauz, G. (2003) Membrane-anchoring and charge effects in the interaction of myelin basic protein with lipid bilayers studied by site-directed spin labeling. *J. Biol. Chem. 278*, 29041–29047.
10. Libich, D. S., and Harauz, G. (2008) Solution NMR and CD spectroscopy of an intrinsically disordered, peripheral membrane protein: evaluation of aqueous and membrane-mimetic solvent conditions for studying the conformational adaptability of the 18.5 kDa isoform of myelin basic protein (MBP). *Eur. Biophys. J. 37*, 1015–1029.
11. Min, Y., Kristiansen, K, Boggs, J. M., Husted, C., Zasadzinski, J. A., and Israelachvili, J. (2009) Interaction forces and adhesion of supported myelin lipid bilayers modulated by myelin basic protein. *Proc. Natl. Acad. Sci. U.S.A. 106*, 3154–3159.
12. Sedzik, J., Blaurock, A. E., and Hoechli, M. (1985) Reconstituted P2/myelin-lipid multilayers. *J. Neurochem. 45*, 844–852.
13. Bates, I. R., Matharu, P., Ishiyama, N., Rochon, D., Wood, D. D., Polverini, E., Moscarello, M. A., Viner, N. J., and Harauz, G. (2000) Characterization of a recombinant murine 18.5-kDa myelin basic protein. *Protein Expr. Purif. 20*, 285–299.
14. Bates, I. R., Libich, D. S., Wood, D. D., Moscarello, M. A., and Harauz, G. (2002) An Arg/Lys→Gln mutant of recombinant murine myelin basic protein as a mimic of the deiminated form implicated in multiple sclerosis. *Protein Expr. Purif. 25*, 330–341.
15. Uyemura, K., Yoshimura, K., Suzuki, M., and Kitamura, K. (1984) Lipid binding activities of the P2 protein in peripheral nerve myelin. *Neurochem. Res. 9*, 1509–1514.
16. Jones, T. A., Bergfors, T., Sedzik, J., and Unge, T. (1988) The three-dimensional structure of P2 myelin protein. *EMBO J. 7*, 1597–1604.
17. Inglis, H. R., Csurhes, P. A., and McCombe, P. A. (2007) Antibody responses to peptides of peripheral nerve myelin proteins P0 and P2 in patients with inflammatory demyelinating neuropathy. *J. Neurol. Neurosurg. Psychiatry 78*, 419–422.
18. Knoll, W., Natali, F., Peters, J., Nanekar, R., Wang, C., and Kursula, P. (2010) Dynamic properties of a reconstituted myelin sheath. *Spectroscopy* in press.
19. Hammarström, M, Woestenenk, E. A., Hellgren, N., Härd, T., and Berglund, H. (2006) Effect of N-terminal solubility enhancing fusion proteins on yield of purified target protein. *J. Struct. Funct. Genomics 7*, 1–14.
20. Studier, F. W. (2005) Protein production by auto-induction in high density shaking cultures. *Protein Expr. Purif. 41*, 207–234.
21. van den Berg, S., Löfdahl, P. A., Härd, T., and Berglund, H. (2006) Improved solubility of TEV protease by directed evolution. *J. Biotechnol. 121*, 291–298.
22. Barrera, N. P., Ormond, S. J., Henderson, R. M., Murrell-Lagnado, R. D., and Edwardson, J. M. (2005) Atomic force microscopy imaging demonstrates that P2X2 receptors are trimers but that P2X6 receptor subunits do not oligomerize. *J. Biol. Chem. 280*, 10759–10765.
23. Durchschlag, H., and Zipper, P. (1997) Calculation of partial specific volumes and other volumetric properties of small molecules and polymers. *J. Appl. Crystallogr. 30*, 803–807.
24. Grant, E. H. (1957) The dielectric method of estimating protein hydration. *Phys. Med. Biol. 2*, 17–28.
25. Majava, V., Wang, C., Myllykoski, M., Kangas, S. M., Kang, S. U., Hayashi, N., Baumgartel, P., Heape, A. M., Lubec, G., and Kursula, P. (2010) Structural analysis of the complex between calmodulin and full-length myelin basic protein, an intrinsically disordered molecule. *Amino Acids* in press.
26. Lawrence, J. C., Saslowsky, D. E., Edwardson, J. M., and Henderson, R. M. (2003) Real-time analysis of the effects of cholesterol on lipid raft behavior using atomic force microscopy. *Biophys. J. 84*, 1827–1832.
27. Frederix, P. L. T. M., Bosshart, P. D., and Engel, A. (2009) Atomic force microscopy of biological membranes. *Biophys. J. 96*, 329–338.
28. De Felici, M., Felici, R., Ferrero, C., Tartari, A., Gambaccini, M., and Finet, S. (2008) Structural characterization of the human cerebral myelin sheath by small angle X-ray scattering. *Phys. Med. Biol. 53*, 5675–5678.
29. Moscarello, M. A., Wood, D. D., Ackerley, C., and Boulias, C. (1994) Myelin in multiple sclerosis is developmentally immature. *J. Clin. Invest. 94*, 146–154.
30. Wood, D. D., Bilbao, J. M., O'Connors, P., and Moscarello, M. A. (1996) Acute multiple sclerosis (Marburg type) is associated

with developmentally immature myelin basic protein. *Ann. Neurol. 40*, 18–24.
31. Saher, G., Brügger, B., Lappe-Siefke, C., Möbius, W., Tozawa, R., Wehr, M. C., Wieland, F., Ishibashi, S., and Nave, K. A. (2005) High cholesterol level is essential for myelin membrane growth. *Nat. Neurosci. 8*, 468–475.
32. Riccio, P., Zito, F., Fasano, A., Liuzzi, G. M., Lolli, F., Polverini, E., and Cavatorta, P. (1998) Purification of bovine P2 myelin protein with bound lipids. *Neuroreport 9*, 2769–2773.
33. Jo, E., and Boggs, J. M. (1995) Aggregation of acidic lipid vesicles by myelin basic protein: dependence on potassium concentration. *Biochemistry 34*, 13705–13716.
34. Surewicz, W. K., Epand, R. M., Epand, R. F., Hallett, F. R., and Moscarello, M. A. (1986) Modulation of myelin basic protein-induced aggregation and fusion of liposomes by cholesterol, aliphatic aldehydes and alkanes. *Biochim. Biophys. Acta 863*, 45–52.
35. ter Beest, M. B., and Hoekstra, D. (1993) Interaction of myelin basic protein with artificial membranes. Parameters governing binding, aggregation and dissociation. *Eur. J. Biochem. 211*, 689–696.
36. Rosetti, C. M., Maggio, B., and Oliveira, R. G. (2008) The self-organization of lipids and proteins of myelin at the membrane interface. Molecular factors underlying the microheterogeneity of domain segregation. *Biochim. Biophys. Acta 1778*, 1665–1675.
37. Rosetti, C. M., Maggio, B., and Wilke, N. (2009) Micron-scale phase segregation in lipid monolayers induced by myelin basic protein in the presence of a cholesterol analog. *Biochim. Biophys. Acta* in press.
38. DeBruin, L. S., Haines, J. D., Wellhauser, L. A., Radeva, G., Schonmann, V., Bienzle, D., and Harauz, G. (2005) Developmental partitioning of myelin basic protein into membrane microdomains. *J. Neurosci. Res. 80*, 211–225.
39. DeBruin, L. S., and Harauz, G. (2007) White matter rafting - membrane microdomains in myelin. *Neurochem. Res. 32*, 213–228.
40. Musse, A. A., Gao, W., Rangaraj, G., Boggs, J. M., and Harauz, G. (2009) Myelin basic protein co-distributes with other PI(4,5)P2-sequestering proteins in Triton X-100 detergent-resistant membrane microdomains. *Neurosci. Lett. 450*, 32–36.
41. Trapp, B. D., Itoyama, Y., MacIntosh, T. D., and Quarles, R. H. (1983) P2 protein in oligodendrocytes and myelin of the rabbit central nervous system. *J. Neurochem. 40*, 47–54.
42. Dupouey, P., Jacque, C., Bourre, J. M., Cesselin, F., Privat, A., and Baumann, N. (1979) Immunochemical studies of myelin basic protein in shiverer mouse devoid of major dense line of myelin. *Neurosci. Lett. 12*, 113–118.
43. Privat, A., Jacque, C., Bourre, J. M., Dupouey, P., and Baumann, N. (1979) Absence of the major dense line in myelin of the mutant mouse "shiverer". *Neurosci. Lett. 12*, 107–112.
44. Mikoshiba, K., Takamatsu, K., and Tsukada, Y. (1983) Peripheral nervous system of shiverer mutant mice: developmental change of myelin components and immunohistochemical demonstration of the absence of MBP and presence of P2 protein. *Brain Res. 283*, 71–79.
45. Winter, J. (1982) Shiverer peripheral myelin contains P2. *Nature 298*, 471–472.
46. Sawaishi, Y., Hayasaka, K., Goto, A., Kawamura, K., Ishiguro, S., Sugai, K., Nonaka, I., Uyemura, K., and Takada, G. (1995) Congenital hypomyelination neuropathy: decreased expression of the P2 protein in peripheral nerve with normal DNA sequence of the coding region. *J. Neurol. Sci. 134*, 150–159.